

Session 2A1

Waves on Metamaterial Elements and Their Applications

Subwavelength Tunneling of Electromagnetic Waves	
<i>H. Wen (The University of British Columbia, Canada); B. Hou (The Hong Kong University of Science and Technology, China); W. J. Wen (The Hong Kong University of Science and Technology, China); ...</i>	446
Reflection at the Boundary of Two Periodic Media: a Generic Approach Applicable to Metamaterials	
<i>L. Solymar (Imperial College, UK); R. R. A. Syms (Imperial College, UK);</i>	447
Waves on Coupled Lines of Resonant Metamaterial Elements: Theory and Experiments	
<i>A. Radkouvskaya (M.V. Lomonosov Moscow State University, Russia); O. Sydoruk (University of Osnabrück, Germany); E. Shamonina (University of Osnabrück, Germany); C. J. Stevens (University of Oxford, UK); D. J. Edwards (University of Oxford, UK); L. Solymar (Imperial College, UK);</i>	448
Quasi-static Waves on Resonant Elements in Non-chiral Periodic Media and Metamaterials: a Historical Survey	
<i>L. Solymar (Imperial College London, UK); E. Shamonina (University of Osnabrück, Germany);</i>	449
Wave Propagation in Grounded Dielectric Slabs with Double Negative Metamaterials	
<i>W. Shu (Iowa State University, USA); J. M. Song (Iowa State University, USA);</i>	450
On the Microstrip Characterization of Artificial Magneto-dielectric Structures	
<i>C. R. Simovski (Helsinki University of Technology, Finland); P. Ikonen (Helsinki University of Technology, Finland); S. Tretyakov (Helsinki University of Technology, Finland);</i>	455
Traveling Waves along the Metasolenoid	
<i>L. Jylhä (Helsinki University of Technology, Finland); S. Maslovski (Helsinki University of Technology, Finland); S. Tretyakov (Helsinki University of Technology, Finland);</i>	456
Plasmonic-polaritonic Photonic-prystal Superlattices as Left-handed Metamaterials	
<i>V. Yannopapas (University of Patras, Greece); A. Moroz (Wave-scattering.com, Germany);</i>	457
Electroinductive Waves on Chains of Resonators	
<i>M. Beruete (Universidad Pública de Navarra, Spain); M. J. Freire (University of Seville, Spain); R. Marqués (Universidad de Sevilla, Spain); F. J. Falcone (Universidad Pública de Navarra, Spain); J. D. Baena (Universidad de Sevilla, Spain);</i>	458
New Experimental Results and Physical Interpretation of a Near-field Planar Magneto-inductive Lens for 3D-subwavelength Imaging	
<i>M. J. Freire (University of Seville, Spain); R. Marques (University of Seville, Spain); J. D. Baena (University of Seville, Spain);</i>	459
Analysis and Visualization of Fields and Waves inside a PEMC Waveguide	
<i>A. H. Sihvola (Helsinki University of Technology, Finland); I. V. Lindell (Helsinki University of Technology, Finland); M. Pitkonen (Helsinki University of Technology, Finland);</i>	460

Subwavelength Tunneling of Electromagnetic Waves

H. Wen¹, B. Hou², and W. J. Wen²

¹The University of British Columbia, Canada

²The Hong Kong University of Science and Technology, China

Under certain conditions, the transmission of electromagnetic waves through subwavelength metallic meshes was enhanced. The metallic mesh (hereby referred to as layer *B*) is sandwiched between two identical layers in three configurations: split ring arrays, metallic plates with periodic fractal slots, and plastic plates with periodic metallic fractals. The *split rings/metallic mesh/split rings* structure demonstrates some unique electromagnetic (EM) characteristics. It is found that the transmittances of EM waves are significantly enhanced at certain frequencies near the stop bands of the split rings. While the metallic plates with periodic fractal slots (layer *A*) and plastic plates with periodic fractals (layer *C*) are a complementary pair (ie an inverse version of each other), in an *ABA* or *CBC* configuration, the composite is found to exhibit multiple transmission peaks which do not appear when layer *B* alone is used. The phenomena of subwavelength tunneling is caused by electromagnetic enhancement at and between the interfaces of the different layers, induced by local resonances of the two outer plates. The simulations indicate that, for the *split rings/metallic mesh/split rings* structure, two different physical mechanisms are responsible for the transmissions: negative refractive index effect, and electromagnetic wave tunneling when EM waves penetrate through negative permittivity substrates sandwiched between two high permittivity slabs. For the *ABA* and *CBC* configurations, the nature of the resonance, electrical or magnetic, is a determinant of locating the transmission peak of the composite, either on the left or the right of the sandwiching layer.

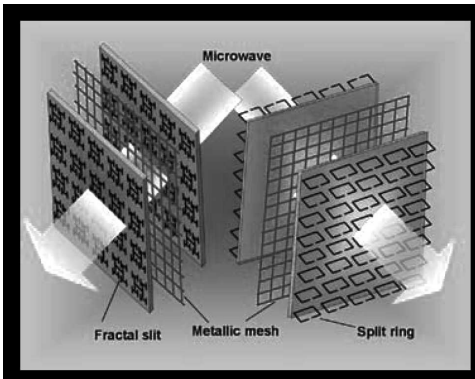


Figure 1: The structural configurations of sandwiched EM metamaterials.

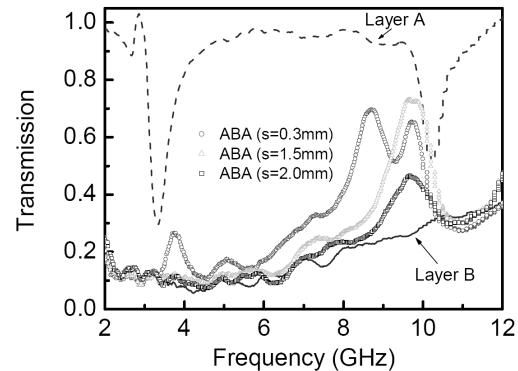


Figure 2: The measured normal transmissions of layer A and B as well as the ABA layers at various separations.

Reflection at the Boundary of Two Periodic Media: a Generic Approach Applicable to Metamaterials

L. Solymar and R. R. A. Syms
Imperial College, UK

One of the central problems of metamaterials research is concerned with the incidence of a plane electromagnetic wave upon a periodic medium [1]. A particularly simple solution, by neglecting the transition layer and higher order modes, for the reflection coefficient has been recently obtained by Tretyakov [2] for the one-dimensional case. An alternative approach to reflection at the boundary of two two-dimensional periodic media consisting of coupled optical waveguides was presented by Syms [3] in the 1980s. His basic idea was to write the recursion equation across the boundary (taking two columns on each side), assume the solution in the form of an incident, a reflected and a transmitted waves and treat interaction between nearest neighbours only. The latter approach is adopted in the present paper to derive generic reflection and transmission coefficients valid for a variety of periodic media which can be described by the nearest neighbour approximation. To show the generality of the expressions examples are given for acoustic waves, plasma waves on nanoparticles (both longitudinal and transverse polarisations), waves on loaded dipoles (both in the axial and in the side-by-side configuration) and magnetoinductive waves on magnetically coupled resonant metamaterial elements (both axial and planar configurations). Potential applications will be discussed

REFERENCES

1. Smith, D. R., W. J. Padilla, D. C. Vier, S. C. Nemat-Nasser, and S. Schultz, *Phys. Rev. Lett.*, Vol. 81, 4184, 2000.
2. Tretyakov, S., *Analytical modeling in applied electromagnetics*, Artech House, Boston, 2000.
3. Syms, R. R. A., "Perturbation analysis of nearly uniform coupled waveguide arrays," *Appl. Opt.*, Vol. 25, 2988-2995, 1986.

Waves on Coupled Lines of Resonant Metamaterial Elements: Theory and Experiments

A. Radkovskaya

M.V. Lomonosov Moscow State University, Russia

O. Sydoruk and E. Shamonina

University of Osnabrück, Germany

C. J. Stevens and D. J. Edwards

University of Oxford, UK

L. Solymar

Imperial College, UK

The coupling and the resulting power transfer between two parallel magnetoinductive waveguides consisting of resonant metamaterial elements were first discussed by Shamonina and Solymar [1]. It was shown that in the lossless case full power transfer is possible between the two waveguides. A particularly interesting case arises when the two waveguides are shifted relative to each other parallel to their axes. At its most general the theory is formulated in terms of five mutual inductances, i.e., each element is coupled to its nearest neighbour in the same waveguide and to the three nearest elements in the parallel waveguide. The resulting dispersion curves have two branches with a stop band between them. The pass band and the power transfer are shown to be fast varying functions of the shift. It is shown further that the power transfer between the two waveguides may vary as much as 40 dB (minimum transmission when the frequency of operation appears to be in the stop band) so that the effect can serve as an efficient switch.

The experiments are performed in the frequency range of 0.3–0.9 GHz using two waveguides parallel to each other consisting of spiral resonant elements in the planar configuration. The first element of waveguide 1 was excited from below by a small loop protruding at the end of a coaxial cable. The receiver consisting of a similar loop was scanned above waveguide 2 measuring the magnetic field at positions corresponding to the centres of the elements. The measured values of the current distribution in waveguide 2 and the measured power transfer between the waveguides are shown to be in good agreement with the theoretical predictions.

REFERENCES

1. Shamonina, E. and L. Solymar, *J. Phys. D: Appl. Phys.*, Vol. 37, 362, 2004.

Quasi-static Waves on Resonant Elements in Non-chiral Periodic Media and Metamaterials: a Historical Survey

L. Solymar
Imperial College, UK

E. Shamonina
University of Osnabrück, Germany

Due to the interest in filters and in slow-wave-structures for microwave tubes several researchers derived dispersion characteristics and discussed their applications both for one-dimensional and two-dimensional cases. The existence of both forward and backward waves were shown, and the relationship between phase and group velocities were examined. This early work done in the 50s and 60s by Mourier [1], Atabekov [2] and Silin [3] will be discussed followed by plasma waves on nanoparticles as presented by Quinton et al. [4], Brongersma et al. [5], and Weber and Ford [6]. Similar waves were shown to be able to propagate along loaded, electrically coupled metallic rods (called electric dipoles in this context) [7], or along a set of magnetically coupled loops [8,9]. Due to their origin these latter waves were called magnetoinductive waves. These additional waves may be excited by an incident electromagnetic wave but they are not dependent on them. They have a separate existence. The similarities and differences between the various waves will be stressed and possible applications [9–13] including near field imaging and near field manipulation such as waveguiding or focusing will be discussed.

REFERENCES

1. Mourier, G., "Circuits a structure periodique a deux et trois dimensions. Applications possibles aux tubes a ondes progressive," *L'Onde Electrique*, Vol. 38, 95–100, 1958.
2. Atabekov, G. I., *Linear Network Theory*, Pergamon Press, Oxford, 1965.
3. Silin, R. A. and V. P. Sazonov, *Slow Wave Structures*, Boston SPA, Eng, National Lending Library for Science and Technology, 1971.
4. Quinton, M., A. Leitner, J. R. Krenn, and F. R. Aussenegg, *Opt. Lett.*, Vol. 23, 1331, 1998.
5. Brongersma, M. L., J. W. Hartman, and H. A. Atwater, *Phys. Rev. B*, Vol. 62, R16356, 2000.
6. Weber, W. H. and G. W. Ford, *Phys. Rev. B*, Vol. 70, 125429, 2004.
7. Tretyakov, S. A. and A. J. Viitanen, *El. Eng.* Vol. 82, 353, 2000.
8. Shamonina, E., V. A. Kalinin, K. H. Ringhofer, and L. Solymar, *Electron. Lett.* Vol. 38, 371, 2002.
9. Shamonina, E., V. A. Kalinin, K. H. Ringhofer, and L. Solymar, *J. Appl. Phys.*, Vol. 92, 6252, 2002.
10. Freire, M. J., R. Marques, F. Medina, M. A. G. Laso, and F. Martin, *Appl. Phys. Lett.*, Vol. 85, 4439, 2004.
11. Nefedov, I. S. and S. A. Tretyakov, *MOTL*, Vol. 45, 98, 2005.
12. Freire, M. J. and R. Marques, *Appl. Phys. Lett.*, Vol. 86, 182505, 2005.
13. Shamonina, E. and L. Solymar, *J. Phys. D: Appl. Phys.* Vol. 37, 362, 2004.

Wave Propagation in Grounded Dielectric Slabs with Double Negative Metamaterials

W. Shu and J. M. Song
Iowa State University, USA

Abstract—In this paper, the wave propagation in a grounded dielectric slab with double negative (DNG) metamaterials is studied. Dramatically different evanescent surface modes (electromagnetic fields exponentially decay both in air and inside the slab) are observed. They are highly dependent on medium parameters. An infinite number of complex surface modes are found to be existing which have proper field distribution in the air region. The investigations on the Poynting vectors show that they do not carry away energy in both transverse and longitudinal directions.

1. Introduction

The guided dielectric slab with a DNG medium has been studied by several groups. Various novel properties are observed: [1] and [2] found that there are special regions for TM (transverse magnetic) modes where two different propagation constants exist. [3] theoretically considered the properties of a planar two-layered waveguide, whose one layer is a double positive (DPS) medium and the other is a DNG medium. Super slowwaves with extremely short wavelenghtes were found whose fields exponentially decay from the interface of the two slabs inside both layers. These guided modes, termed as evanescent surface modes, were also found by [4] and [5], respectively. P. Baccarelli and his colleague suggested the concept of surface wave suppression that ensures the absence of both ordinary and evanescent surface modes. This is very attractive in view of taking DNG medium as a potential substrate candidate to reduce edge diffraction effects and enhance radiation efficiency for microstrip antennas [6].

However, so far as the authors are aware no study on the complex modes and Poynting vectors has been reported. This makes the mode spectra of DNG media unpleasantly incomplete. In this paper, the authors focus on the properties of the evanescent surface modes and the complex modes, both of which belong to the proper mode spectra of the grounded dielectric slab with a DNG medium. It is found that the evanescent surface modes are highly dependent on the medium parameters and an infinite number of complex modes exists which have exponentially decaying fields in the air region. They are termed complex surface modes. The study on the Poynting vectors shows that they have zero power flows in both transverse and longitudinal directions.

2. Eigen Equations and Graphical Solutions

The structural setup of interest here is a grounded dielectric slab of thickness d (see Figure 1). Region one is a DNG medium and region two is air. It is well known that to ensure a positive stored energy in the dielectric layer, passive DNG media must be dispersive [7]. However, for simplicity we assume that they are isotropic, lossless, and non-dispersive. This assumption is found to be acceptable since a small dispersion of ϵ and μ can satisfy the constraints.

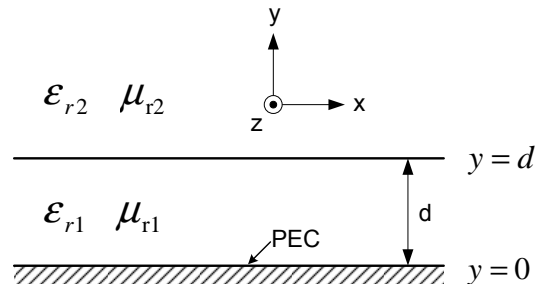


Figure 1: Geometry structure of a grounded dielectric slab with DNG medium ($\epsilon_{r1} < 0, \mu_{r1} < 0$).

Using the well-known transverse resonance method [8], the eigen equations for ordinary ($\gamma_{y1} = jk_{y1}$) real

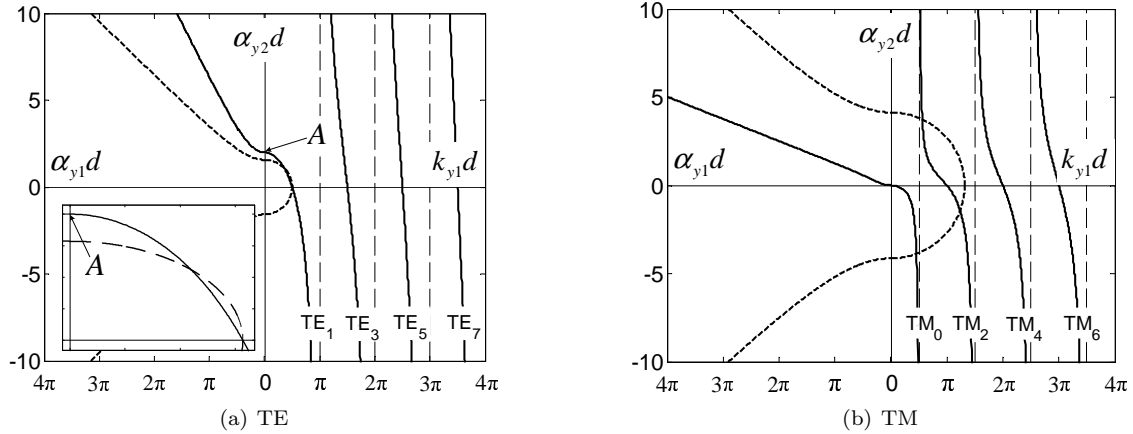


Figure 2: Graphical solutions for TE and TM modes. Solid lines in the first and fourth quadrants represent (1) or (2); solid lines in the second quadrant represent (4) or (5); dashed line in the first and fourth quadrants represents (3); dashed line in the second and third quadrants represents (6). The medium parameters are: $\epsilon_{r1} = -2.5$, $\mu_{r1} = -0.5$, $\epsilon_{r2} = 1$, $\mu_{r2} = 1$.

modes are:

$$\frac{\mu_{r2}}{\mu_{r1}}(k_{y1}d) \cot(k_{y1}d) = -\alpha_{y2}d \quad \text{for TE} \quad (1)$$

$$\frac{\epsilon_{r2}}{\epsilon_{r1}}(k_{y1}d) \tan(k_{y1}d) = \alpha_{y2}d \quad \text{for TM} \quad (2)$$

$$(k_{y1}d)^2 + (\alpha_{y2}d)^2 = (k_0d)^2(\epsilon_{r1}\mu_{r1} - \epsilon_{r2}\mu_{r2}) \quad (3)$$

The eigen equations for evanescent ($\gamma_{y1} = \alpha_{y1}$) real modes are:

$$\frac{\mu_{r2}}{\mu_{r1}}(\alpha_{y1}d) \coth(\alpha_{y1}d) = -\alpha_{y2}d \quad \text{for TE} \quad (4)$$

$$\frac{\epsilon_{r2}}{\epsilon_{r1}}(\alpha_{y1}d) \tanh(\alpha_{y1}d) = -\alpha_{y2}d \quad \text{for TM} \quad (5)$$

$$(\alpha_{y2}d)^2 - (\alpha_{y1}d)^2 = (k_0d)^2(\epsilon_{r1}\mu_{r1} - \epsilon_{r2}\mu_{r2}) \quad (6)$$

where $k_0^2 = \omega^2\mu_0\epsilon_0$. γ_{y1} , γ_{y2} are the y -direction wave constants of the two layers. Their relationship to the longitudinal wave constant (z -direction) γ is written as:

$$\gamma_{yi}^2 = -k_0^2\epsilon_{ri}\mu_{ri} - \gamma^2 \quad (i = 1, 2) \quad (7)$$

Graphical representations of the above equations are shown in Figure 2. The mode index notation here follows [9]. Notice that in the first and second quadrants, α_{y2} is positive and the fields exponentially decay in the air region (proper); in the third and fourth quadrants, α_{y2} is negative and the fields exponentially increase in the air region (improper). The x -axis is divided into two segments. The right half is for $k_{y1}d$ and the fields in the dielectric layer are sine/cosine standing waves (ordinary), while the left half is for $\alpha_{y1}d$ and the fields in the dielectric layer are exponentially distributed (evanescent). Therefore, the intersection in the second quadrant represents the *proper evanescent* surface mode, which does not exist for a DPS medium.

Another important difference for a DNG medium that can be read from Figure 2 is that the ordinary surface mode solutions are no longer monotonic. It is clear from the subfigure in the left corner of Figure 2(a) that there are two intersections as the radius of the dashed circle decreases, which corresponds to a decrease of frequency. Once the circle has only one tangential point with the solid line, further decreasing frequency will cause this mode to be cutoff. The same thing happens to TM modes in Figure 2(b) in a more obvious way. These two possible modes have two different power flow distributions. One has more power flowing in the air region than in the dielectric region, making the total power flow in the same direction as the phase velocity. The other is in the opposite way and displays a backward property. More details on the Poynting vectors are addressed in Section 4.

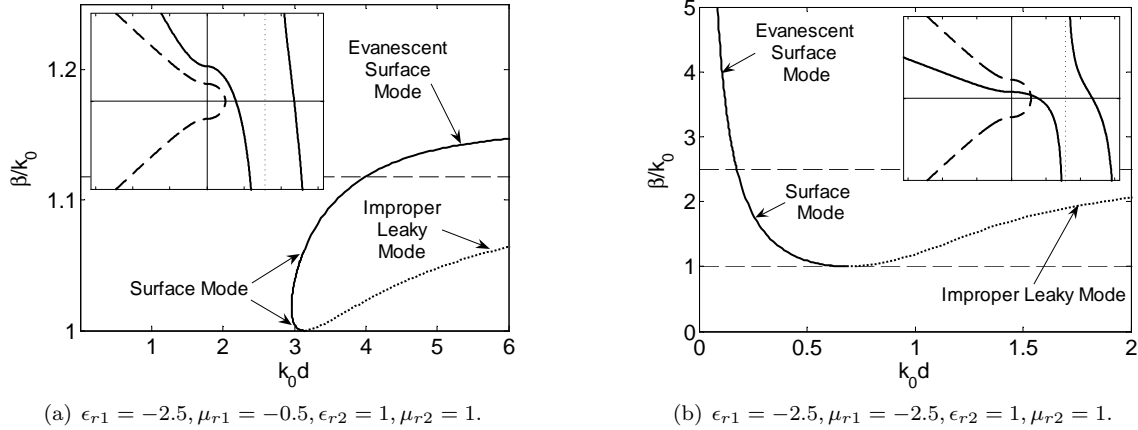


Figure 3: Two possible dispersion curves for TE proper surface modes (solid lines) and TE improper leaky modes (dotted lines). The dashed line, representing $\sqrt{\epsilon_{r1}\mu_{r1}}$, is the watershed for evanescent surface mode and ordinary surface modes.

3. Evanescent Surface Mode

As stated in Section 2, the proper evanescent surface mode does exist with a DNG medium. It is the intersection in the second quadrant. The normalized effective dielectric constant $\epsilon_{eff} = (\beta/k_0)^2$ for evanescent surface mode is larger than both $\epsilon_{r1}\mu_{r1}$ and $\epsilon_{r2}\mu_{r2}$. Therefore the transverse propagation constant in the dielectric layer $\gamma_{y1} = \sqrt{-k_0^2\epsilon_{r1}\mu_{r1} - \gamma^2} = k_0\sqrt{\epsilon_{eff} - \epsilon_{r1}\mu_{r1}}$ is a pure real number. The electromagnetic fields are no longer sine/cosine standing waves, but have the form of $Ae^{-\alpha_{y1}y} + Be^{\alpha_{y1}y}$.

It is found, however, that the dispersion curves for evanescent surface modes are very complicated, and they are highly dependent on the medium parameters. Figure 3 shows two dispersion diagrams for TE₁ mode with different medium parameters. The dispersion curves represent the intersection points of the dashed line and the first solid branch in Figure 2(a), including the part in the second quadrant. The solid line in Figure 3 is for proper modes, while the dotted line is for improper mode, which is the set of intersections in the fourth quadrant in Figure 2(a). The dashed lines in both figures depict the value of $\sqrt{\epsilon_{r1}\mu_{r1}}$. They are the watersheds by which one can tell the evanescent surface mode from ordinary ones.

In Figure 3(a), the evanescent surface mode has low cutoff frequency. As the frequency increases, the ordinary surface mode becomes an evanescent surface mode and its effective dielectric constant, ϵ_{eff} , keeps increasing. In Figure 3(b), however, the situation is reversed. The evanescent surface mode has a high cutoff frequency above which it becomes the ordinary surface mode. At the low frequency range, the evanescent surface mode has an extremely large ϵ_{eff} , which decreases rapidly as the frequency increases. One can refer to the subfigures of Figure 3 to check the validations. The reason for such dramatically different dispersion curves is that with DNG metamaterials, one can not only make ϵ and μ simultaneously negative but also let their absolute values be less than one [5]. From (1) and Figure 2(a), it is easy to see that the crossing point of the first solid branch TE₁ with the x -axis is fixed at $(\pi/2, 0)$, while the crossing point with the y -axis noted as ‘A’ in Figure 2(a) is $(0, |\mu_{r2}/\mu_{r1}|)$. With a conventional DPS medium, μ_{r1} is always equal to unity, or slightly greater or smaller than unity as in the case of paramagnetic or diamagnetic materials. With metamaterials, however, μ_{r1} is not confined near unity any more and the intercept with the y -axis may change a lot. This change affects the possible intersections of the first solid line and the dashed line in Figure 2(a) and finally results in dramatically different dispersion curves.

4. Complex Surface Modes and Poynting Vectors

It is well known that the complete proper mode spectra for a DPS dielectric slab include discrete surface modes and continuous radiation modes, both of which are real modes [8]. With a DNG medium, however, it is proved by the authors that the complex roots of the eigen equations are exclusively on the top Riemann sheet [10]. These solutions, termed complex surface waves, form another set of proper modes since they have exponentially decaying fields in the air region and satisfy the boundary conditions at infinity. Unlike real surface modes, complex surface modes have high cutoff frequencies below which they exist.

Figure 4 shows the dispersion diagrams for both TE and TM modes, including evanescent, ordinary, and

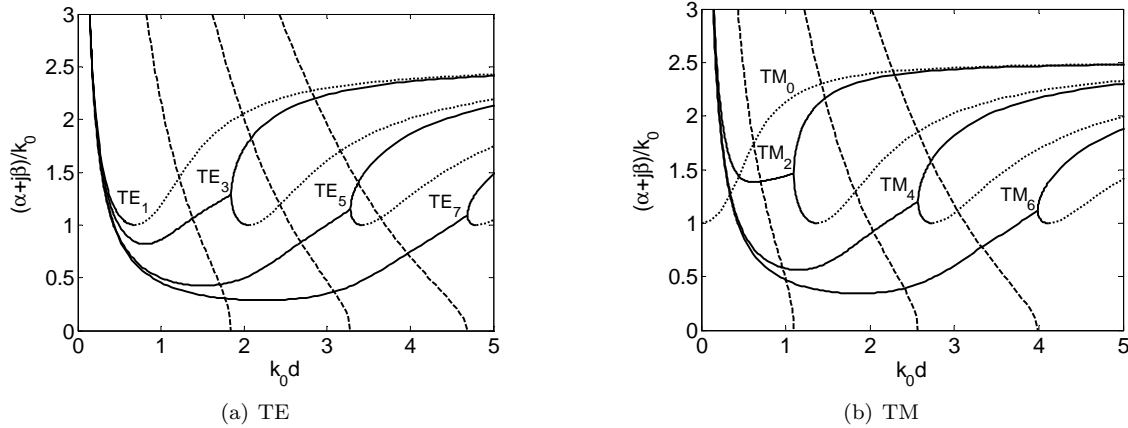


Figure 4: Dispersion diagrams for all modes. Solid line is for normalized β of the proper modes. Dashed line is for normalized α of the proper modes. Dotted line is for normalized β of the improper modes. The medium parameters are: $\epsilon_{r1} = -2.5$, $\mu_{r1} = -2.5$, $\epsilon_{r2} = 1$, $\mu_{r2} = 1$.

complex surface modes. Also included are improper leaky modes drawn as dotted lines. When the frequency is much lower than the first cutoff frequency of the real modes, all complex modes exist with very high normalized α and β . As the frequency increases, β/k_0 tends to decrease rapidly within a very narrow frequency range; after that it increases slowly till its cutoff frequency. Notice it is not monotonic and the value of β/k_0 can be less than unity, which is a notable difference compared with evanescent and ordinary surface modes. The curve of α/k_0 , however, monotonically decreases very fast as the frequency increases. At the cutoff point, α reaches zero and β becomes the starting point of the real mode. The real surface mode bifurcates into two branches from this point. One branch has an increasing β/k_0 as the frequency goes high, while the other has a decreasing β/k_0 , which will reach unity shortly. This property is expected from Figure 2. Further increasing frequency makes β/k_0 of the second branch begin to rise. However, it is no longer a proper mode.

It is found that the complex surface modes have zero power flows [10]. To derive the Poynting vector for complex modes, γ_{y1} , γ_{y2} , and γ are assumed to be:

$$\begin{aligned}\gamma_{y1} &= a + jb \\ \gamma_{y2} &= u + jv \\ \gamma &= \alpha + j\beta\end{aligned}\quad (8)$$

The Poynting vector is written as

$$S_z^{\text{TE}} = \frac{1}{2} E_x H_y^* = \frac{|A|^2}{2} \begin{cases} S_{z1}^{\text{TE}}, & \text{for } 0 < y < d \\ S_{z2}^{\text{TE}}, & \text{for } y \geq d \end{cases} \quad (9)$$

where A is the electric field intensity and S_{z1}^{TE} and S_{z2}^{TE} are as follows:

$$S_{z1}^{\text{TE}}(y, z) = \frac{\beta + j\alpha}{2\omega\mu_{r1}} e^{-2\alpha z} [\cosh(2ay) - \cos(2by)] \quad (10)$$

$$S_{z2}^{\text{TE}}(y, z) = \frac{\beta + j\alpha}{2\omega\mu_{r2}} e^{-2u(y-d) - 2\alpha z} [\cosh(2ad) - \cos(2bd)] \quad (11)$$

Figure 5 shows the dispersion diagram and the integral results of Poynting vector for the TE_3 mode. In Figure 5(a), only the complex mode exists (branch ‘A’) when the frequency is lower than the cutoff frequency of the real surface mode. The zero power flow in z -direction in Figure 5(b) shows that the complex surface mode does not carry away any energy. As the frequency increases, the real surface mode begins. The top branch (branch ‘B’) of the real mode carries a negative power flow and shows backward properties. When a waveguide operates in this mode, its fields are largely confined inside the dielectric layer. The bottom branch (branch ‘C’) of the real mode carries a positive power flow and its fields extend far away in the air region. Further increasing frequency causes the fields in the air region to decay more slowly, and eventually reach infinity. At that point, the radiation boundary conditions are violated and the mode becomes improper.

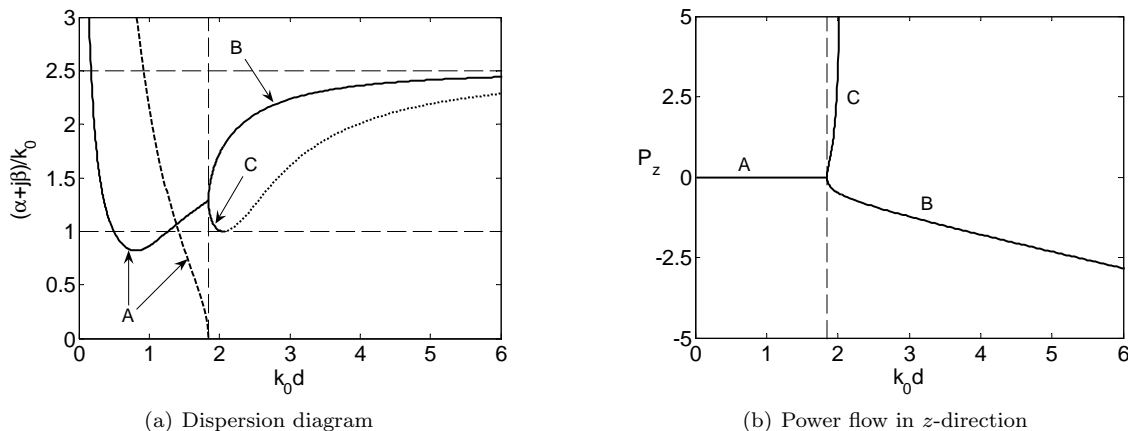


Figure 5: Dispersion diagram and the power flow in z -direction for TE modes. ‘A’ is for complex surface mode; ‘B’ is for top branch of the real surface mode; ‘C’ is for bottom branch of the real surface mode. The medium parameters are: $\epsilon_{r1} = -2.5$, $\mu_{r1} = -2.5$, $\epsilon_{r2} = 1$, $\mu_{r2} = 1$.

5. Conclusion

In this paper, an investigation on the mode properties of a grounded dielectric slab with a DNG medium has been dealt with. The graphical method is used to find the possible real roots. Dramatically different dispersion curves of evanescent surface modes are observed, showing that they are very sensitive to the material parameters. It is found that there is an infinite number of complex surface modes with a DNG medium and they do not carry away energy. Although the considered medium here is idealized and currently cannot be realized, the results of this paper still unveil some exotic properties as well as potential applications of the metamaterials.

REFERENCES

1. Cory, H. and A. Barger, “Surface-wave propagation along a metamaterial slab,” *Microwave Opt. Technol. Lett.*, Vol. 38, 392–395, Sept. 2003.
2. Dong, H. and T. X. Wu, “Analysis of discontinuities in double-negative (DNG) slab waveguides,” *Microwave Opt. Technol. Lett.*, Vol. 39, 483–488, Dec. 2003.
3. Nefedov, I. S. and S. A. Tretyakov, “Waveguide containing a backward-wave slab,” *Radio Sci.*, Vol. 38, 1101–1109, 2003.
4. Wu, B.-I., T. M. Grzegorzczak, Y. Zhang, and J. A. Kong, “Guided modes with imaginary transverse wave number in a slab waveguide with negative permittivity and permeability,” *J. Appl. Phys.*, Vol. 93, 9386–9388, Jun. 2003.
5. Shadrivov, I. W., A. A. Sukhorukov, and Y. S. Kivshar, “Guided modes in negative-refractive-index waveguides,” *Phys. Rev. E, Stat. Phys. Plasmas Fluids Relat. Interdiscip. Top.*, Vol. 67, 057602–057602, May 2003.
6. Baccarelli, P., P. Burghignoli, F. Frezza, A. Galli, P. Lampariello, G. Lovat, and S. Paulotto, “Fundamental modal properties of surface waves on metamaterial grounded slabs,” *IEEE Trans. Microwave Theory Tech.*, Vol. 53, 1431–1442, Apr. 2005.
7. Smith, D. R. and N. Kroll, “Negative refractive index in left-handed materials,” *Phys. Rev. Lett.*, Vol. 85, 2933–2936, Oct. 2000.
8. Collin, R. E., *Field Theory of Guided Waves*, 2nd, Ed. Piscataway, IEEE Press, NJ, 1991.
9. Balanis, C. A., *Advanced Engineering Electromagnetics*, John Wiley & Sons, NJ, 1989.
10. Shu, W. and J. M. Song, “On the properties of a grounded dielectric slab with double negative metamaterials,” *IEEE Trans. Microwave Theory Tech.*, to be submitted.

On the Microstrip Characterization of Artificial Magneto-dielectric Structures

C. R. Simovski^{1,2}, P. Ikonen¹, and S. Tretyakov¹

¹Helsinki University of Technology, Finland

²St. Petersburg Institute of Fine Mechanics and Optics, Russia

Wideband measurement methods are needed for extracting effective material parameters of artificially engineered composite materials to enable further development and optimization of these materials. It is obvious that resonator based measurement techniques fail to fulfill the ultimate goal of wideband characterization. Therefore, waveguide measurement methods become necessary. Depending on the characterized material sample, usually two basic guiding structures are utilized: small scatterers or homogeneous blocks of material can be measured using a parallel-plate waveguide or a (quasi-)TEM transmission line, usually a normal microstrip line. Building a parallel-plate waveguide operating at low frequencies (1–3 GHz) is practically difficult, thus, we propose to use a microstrip line. In this presentation we demonstrate an experimental characterization process targeted to extract the material parameters of a uniaxial artificial magneto-dielectric sample with resonant properties. We extract the parameters from measured S-parameters of loaded and empty microstrip line. It is shown that the proposed technique is suitable for characterizing the properties of the material over a rather wide frequency range excluding the thickness resonance bands. We use the comparison of S-parameters of the material block under test and a reference block with known permittivity and no magnetic properties. The novelty of our work is related with modifications of the known characterization methods. These modifications are required when the following three factors simultaneously disturb the characterization procedure:

1. The network analyzer cannot be calibrated with respect to the actual input ports but with respect to the cable connectors, because the properties of two cable connectors and therefore the electric distance between the calibration point and the input ports is unknown.
2. The wavelength in the empty waveguide is not exactly equal to that of free space, and we do not know the possible error.
3. The reference dielectric block with known material parameters (that is used in the proposed comparative method) does not fill the effective cross section of the microstrip line completely.

Traveling Waves along the Metasolenoid

L. Jylhä, S. Maslovski, and S. Tretyakov
Helsinki University of Technology, Finland

A new magnetic particle called “metasolenoid” was introduced in [1, 2], see Figure 1. It consists of a stack of closely packed metallic single split-ring resonators. In the lowest-order resonant mode the metasolenoid can be used as a magnetic inclusion [1], but in its higher order modes it can be used as a high-quality resonator [2]. At higher modes, the magnetic field is mostly concentrated inside the solenoid, where are no metallic parts. The field distribution is quite similar to that inside volume resonators. Therefore, the quality factor of a metasolenoid can be much higher than the quality factor of an ordinary microstrip resonator.

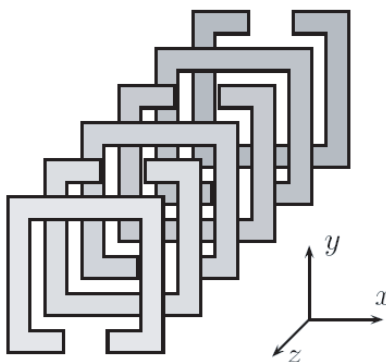


Figure 1: Geometry of the metasolenoid.

In this study, we focus on the use of the metasolenoid as a waveguiding structure. Eigenmodes in a waveguide made of coupled capacitively loaded wire loops were studied also in [3, 4], but there only the interaction between the neighboring loops was taken into account. Such approach is valid only if the separation between the loops is of order of the loop radius or larger, i.e., when the interaction between the loops is weak. In this study, the interaction between the rings that are not neighbors is also taken into account. Therefore, structures with small separations between the rings can be studied. When the separation between the rings is small, the coupling between them is strong and the waveguide is capable to support slow waves with very short wavelength.

Metasolenoids can find applications in the design of delay lines, filters, and resonant magnetic sensors.

REFERENCES

1. Maslovski, S., P. Ikonen, I. Kolmakov, S. Tretyakov, and M. Kaunisto, “Artificial magnetic materials based on the new magnetic particle: metasolenoid,” *Progress in Electromagnetics Research*, Vol. 54, 61–81, 2005.
2. Jylhä, L., S. Maslovski, and S. Tretyakov, “High-order resonant modes of a metasolenoid,” *Journal of Electromagnetic Waves and Applications*, Vol. 19, No. 10, 1327–1342, 2005.
3. Shamonina, E., V. A. Kalinin, K. H. Ringhofer, and L. Solymar, “Magnetoinductive waves in one, two, and three dimensions,” *J. Appl. Phys.*, Vol. 92, 6252, 2002.
4. Shamonina, E. and L. Solymar, “Magneto-inductive waves supported by metamaterial elements: components for a one-dimensional waveguide,” *J. Phys. D: Appl. Phys.*, Vol. 37, 362, 2004.

Plasmonic-polaritonic Photonic-crystal Superlattices as Left-handed Metamaterials

V. Yannopapas

University of Patras, Greece

A. Moroz

Wave-scattering.com, Germany

Left-handed metamaterials come in two basic types, namely those based on purely dielectric periodic structures, or as periodic metallic microstructures exhibiting electric and magnetic resonances [1]. The purely dielectric metamaterials are characterised by rather low wavelength-to-structure ratio (typically less than 2:1). On the other hand, the metamaterials based on metallic microstructures, the most prominent example of which are those consisting of split ring resonators (SRRs) and wires, are truly subwavelength structures with wavelength-to-structure ratio at least 5:1. Here, we present a new set of artificial structures which can exhibit a negative refractive index band in excess of 6% in a broad frequency range from deep infrared to terahertz range [2]. The structures are composites of two different kinds of non-overlapping spheres, one made from inherently non-magnetic polaritonic and the other from a Drude-like material. The polaritonic spheres are responsible for the existence of negative effective magnetic permeability whilst the Drude-like spheres are responsible for negative effective electric permittivity. The resulting negative refractive index structures are truly subwavelength structures with wavelength-to-structure ratio 14:1, which appears almost by 50% higher than it has been achieved so far. Our results are explained in the context of the extended Maxwell - Garnett theory [3] and reproduced by the calculations based on the layer Korringa-Kohn-Rostoker method, an ab initio multiple scattering theory [4, 5].

REFERENCES

1. Pendry, J. B., "Negative refraction," *Contemp. Phys.*, Vol. 45, No. 3, 191–202, 2004.
2. Yannopapas, V. and A. Moroz, "Negative refractive index metamaterials from inherently non-magnetic metamaterials for deep infrared to terahertz frequency ranges," *J. Phys.: Condens. Matter*, Vol. 17, No. 25, 3717–3734, 2005.
3. Ruppin, R., "Evaluation of extended Maxwell-Garnett theories," *Opt. Commun.*, Vol. 182, Nos. 4–6, 273–279, 2000.
4. Stefanou, N., V. Yannopapas, and A. Modinos, "Heterostructures of photonic crystals: frequency bands and transmission coefficients," *Comput. Phys. Commun.*, Vol. 113, No. 1, 49–77, 1998.
5. Stefanou, N., V. Yannopapas, and A. Modinos, "MULTEM 2: A new version of the program for transmission and band-structure calculations of photonic crystals," *Comput. Phys. Commun.*, Vol. 132, Nos. 1-2, 189–196, 2000.

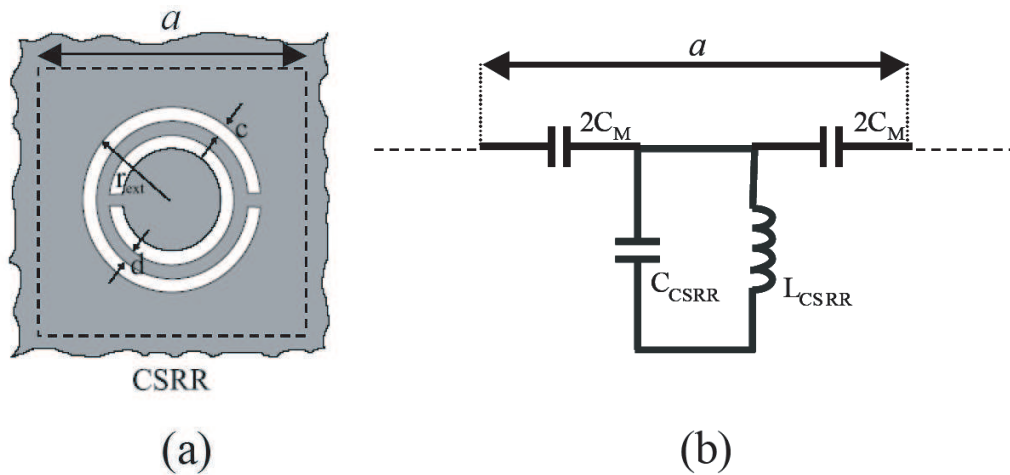
Electroinductive Waves on Chains of Resonators

M. Beruete¹, M. J. Freire², R. Marqués², F. J. Falcone¹, and J. D. Baena²

¹Universidad Pública de Navarra, Spain

²Universidad de Sevilla, Spain

A new kind of waves supported by chains of resonators drilled on a metallic substrate is presented. Propagation of energy comes as a consequence of the electric coupling between these resonators. Therefore, these waves are termed as electroinductive waves (EIWs). They can be interpreted as the dual counterpart of the so called magnetoinductive waves (MIWs) [1–3], which are due to the mutual inductance between chains of resonators. The unit cell of the analyzed structure is formed by the dual or “complementary” (in Babinet’s sense) particle of the split ring resonator (CSRR), recently reported in [4]. This unit cell, as well as its circuit model, is shown in the Figure. In order to show the existence and excitation of the reported EIWs, analytical calculations, electromagnetic simulations and experiments have been carried out. Both, simulations and experiments show a very good agreement with the analytical model.



REFERENCES

1. Shamonina, E., V. A. Kalinin, K. H. Ringhofer, and L. Solymar, *Electron. Lett.*, Vol. 38, 371, 2002.
2. Shamonina, E., V. A. Kalinin, K. H. Ringhofer, and L. Solymar, *J. Appl. Phys.*, Vol. 92, 6252, 2002.
3. Shamonina, E. and L. Solymar, *J. Phys. D*, Vol. 37, 362, 2004.
4. Falcone, F., T. Lopetegi, M. A. G. Laso, J. D. Baena, J. Bonache, M. Beruete, R. Marques, F. Martin, and M. Sorolla, *Phys. Rev. Lett.*, Vol. 93, 197401, 2004.

New Experimental Results and Physical Interpretation of a Near-field Planar Magneto-inductive Lens for 3D-subwavelength Imaging

M. J. Freire, R. Marqués, and J. D. Baena
University of Seville, Spain

Near-field sub-wavelength imaging has been proposed in the optical frequency range by using a planar silver slab [1] and in the microwave regime by using a magnetized ferrite slab [2]. In both cases the physical mechanism involving the imaging is the amplification of the evanescent Fourier harmonics of the electromagnetic field coming from the source by means of the excitation of surface waves in the slab interfaces. More recently a near-field lens operating in the microwave regime based on the excitation of surface magnetoinductive (MI) waves in a two-dimensional (2D) planar array of inductively coupled resonators has been reported [3]. The device consists of two parallel 2D arrays of broadside coupled split ring resonators (BCSRR). A loop input antenna is used as field source and a similar output antenna is used to measure the image. The reported device shows 3D super resolution (see Figure 2). After these encouraging results new prototypes were fabricated and a physical interpretation of the results is in progress [4]. The aim of this contribution is to present these new experimental results, altogether with its physical interpretation.

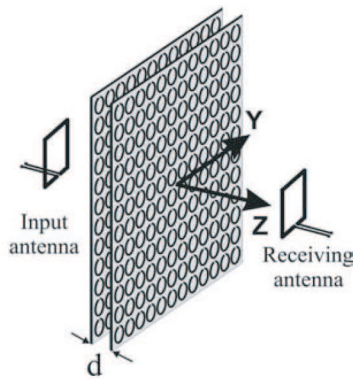


Figure 1: Sketch of the experimental setup.

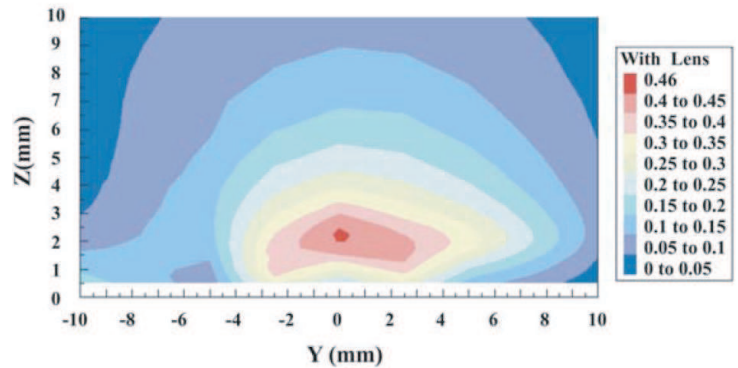


Figure 2: Measurement of the transmission coefficient between the antennas in the device of Figure 1.

REFERENCES

1. Fang, N., H. Lee, C. Sun, and X. Zhang, *Science*, Vol. 308, 534, 2005.
2. Marques, R., F. Mesa, and F. Medina, *App. Phys. Lett.*, Vol. 86, 023505, 2005.
3. Freire, M. and R. Marques, *App. Phys. Lett.*, Vol. 86, 182505, 2005.
4. Marques, R., F. Mesa, M. Freire, and J. D. Baena, *Proc. of the ICECOM05 Conf.*, Dubrownik, Croatia, 2005.

Analysis and Visualization of Fields and Waves inside a PEMC Waveguide

A. H. Sihvola, I. V. Lindell, and M. Pitkonen
Helsinki University of Technology, Finland

The PEMC medium is a special type of metamaterial which is a generalization of the well-known concepts of PEC (perfect electric conducting) and PMC (perfect magnetic conducting) media. Perfect electromagnetic medium is characterized by an admittance-type parameter $M = \cot \vartheta$, and the choices of $\vartheta = 0$ and $\vartheta = \pi/2$ give the PEC and PMC cases, respectively. For the basic properties of PEMC media, see [1–3].

The effect of the PEMC boundary is that the field that is incident on it will suffer a rotation in polarization. Hence it is a non-reciprocal actor in the electromagnetic problem. (In fact, the suggested realizations of PEMC elements require gyrotropic materials; either ferrites or magnetized plasma -type antisymmetric material parameter responses.) As the ordinary metal waveguide serves as a structure where longitudinal propagation is combined with reflection resonances in the transverse direction, we can expect interesting effects to be found in the behavior of electromagnetic fields that are transmitted through a waveguide with walls made of PEMC material.

We have analyzed the electric and magnetic fields in PEMC waveguides for propagating modes. The field structure is obviously dependent on the M parameter and it can be seen to approach uniformly the well-known fields of waveguides with PEC or PMC walls. The effect of finite value of the PEMC parameter M is that the transverse fields are no longer orthogonal, at the walls the electric field has a tangential component and both electric and magnetic fields have longitudinal components, forming paired loops. In the presentation we shall visualize these effects in various ways.

REFERENCES

1. Lindell and Sihvola, *J. Electro. Waves Applic.*, Vol. 19, No. 7, 861–869, 2005.
2. Lindell and Sihvola, *IEEE Trans. Antennas Propagat.*, Vol. 53, No. 9, 3005–3011, September 2005.
3. Lindell and Sihvola, *IEEE Trans. Antennas Propagat.*, 3012–3018.